

## Decay process of photoexcited divacancies in diamond studied by first-principles simulations

Yoshiyuki Miyamoto <sup>\*</sup>*Advanced Power Electronics Research Center, National Institute of Advanced Industrial Science and Technology (AIST)  
Central 2, 1-1-1, Umezono, Tsukuba 305-8568, Japan* (Received 18 May 2023; revised 1 July 2023; accepted 2 August 2023; published 15 August 2023)

Color centers in diamond have attracted much attention as potential quantum photodevices. In contrast to nitrogen vacancy and group-IV-vacancy centers, the optical properties of other thermally stable vacancies have not been thoroughly studied. This work focuses on a divacancy in diamond, and its optical properties were studied by applying first-principles simulation schemes. A structure with two vacancies in the nearest-neighbor sites was chosen as a test case, and calculations of dipole matrix elements by density functional theory found two possible optical excitation paths. According to the electron-ion dynamics calculated by time-dependent density functional theory, one excitation path showed nonradiative decay, suggesting that it would not emit light. The other excitation path seemed to hold its excited state for 500 fs, but the light emission intensity appeared to be weakened. The effect of hydrogen termination of the divacancy was also studied. The current results provide a fundamental understanding of the optical properties of divacancies and should trigger future research into their influence on the properties of color centers in diamond.

DOI: [10.1103/PhysRevMaterials.7.086002](https://doi.org/10.1103/PhysRevMaterials.7.086002)

## I. INTRODUCTION

Improving light emission efficiency is vital for high-performance optical devices. Nonradiative decay of excited carriers decreases light emission efficiency, and vacancy-related defects can cause this decay. Decreasing the number of vacancy-related defects increases the light emission efficiency in semiconductors [1–4] which can be theoretically understood by the perturbation scheme for electron-phonon scattering [5,6]. However, in diamond, some defects can be sources of light emission, such as nitrogen vacancy (NV) centers [7–13] and group-IV vacancy (IV-V) centers [14–20]. In addition to these color centers, diamond contains thermally stable vacancies [21,22], of which divacancies have been identified as stable under heat treatment by measuring luminescence after annealing [23,24]. Divacancies affect the charge states of IV-V centers [19] through the excited carrier dynamics of the divacancy. Hereafter, “divacancy” specifically refers to diamond divacancies.

The electronic structure, optical transition, and decay process of excited states in divacancies have not been studied intensively compared with those in NV and IV-V centers. To examine the decay process by calculating the real-time electron-ion dynamics, the present work uses time-dependent density functional theory (TDDFT) [25], which is a time-dependent version of static density functional theory (DFT) [26,27], and discusses possible optical properties. Although it may be time-consuming, the current approach using the real-time electron-ion dynamics is convenient for extended systems in which electronic levels with different occupations cross to each other.

In this work, the electronic structure of divacancy in the neutral charge state is shown as well as two optical excita-

tion paths with corresponding excitation energies of 2.44 and 2.32 eV. The TDDFT electron-ion dynamics simulations at a lattice temperature of 10 K suggested that the first excitation path shows fast nonradiative decay resulting in direct electron-hole coupling, whereas the second path appeared to remain for at least 500 fs. Furthermore, the first excitation path was annihilated by hydrogen (H) termination in the divacancy, whereas the second path remained. The remaining path shows the excited hole state spreading into the bulk throughout the electron-ion dynamics simulation indicating low light emission efficiency.

The paper is structured as follows. The computational schemes are explained in Sec. II, the results for decay process of the excited carriers of the divacancy are presented in Sec. III, and the concluding remarks are given in Sec. IV.

## II. COMPUTATIONAL SCHEMES

The real-time electron-ion dynamics based on TDDFT was performed within the Ehrenfest approximation [28]. The electron dynamics were numerically computed by solving the time-dependent Kohn-Sham equation [25],

$$i \frac{\partial}{\partial t} \psi_n^{\text{TDDFT}}(\mathbf{r}, t) = H^{KS}(\mathbf{r}, t) \psi_n^{\text{TDDFT}}(\mathbf{r}, t). \quad (1)$$

Here,  $\psi_n^{\text{TDDFT}}(\mathbf{r}, t)$  is the time-dependent version of the Kohn-Sham orbital [27] with band index  $n$ , and the Hamiltonian,  $H^{KS}(\mathbf{r}, t)$ , is constructed with the exchange-correlation potential as a functional of the charge density,  $\rho(\mathbf{r}, t)$ , within the adiabatic approximation. The ion dynamics were treated with Newton’s equation of motion,

$$M_I \frac{\partial^2}{\partial t^2} \mathbf{R}_I(t) = \mathbf{F}_I(t), \quad (2)$$

where  $M_I$ ,  $\mathbf{R}_I$ , and  $\mathbf{F}_I$  denote the mass, position, and force of ion  $I$ , respectively. Force  $\mathbf{F}_I$  used in Eq. (2) was calculated

<sup>\*</sup>yoshi-miyamoto@aist.go.jp

from charge density  $\rho(\mathbf{r}, t)$  and the ionic positions by using the scheme for periodic systems [29] at each time step of the molecular dynamics (MD) coupled with the real-time evolution of electrons by solving the time-dependent Kohn-Sham equation (1).

The excited states were prepared within static DFT as the initial condition of the TDDFT calculation. An approximation for the excited state obtained by promoting electron occupation throughout the self-consistent field (SCF) calculation was used. This approximation is called the  $\Delta$ SCF scheme, and the excitation energy is evaluated by a total-energy difference between the ground and excited states. Throughout the real-time electron-ion dynamics, the occupation numbers of promoted electrons were fixed, but the decay dynamics were monitored as the time evolution of the wave function characteristics of the excited hole. The expectation values of the Kohn-Sham Hamiltonian  $H^{KS}(\mathbf{r}, t)$  were also monitored, which showed the alternation of levels with different electron occupation numbers at the moment of the decay. This scheme has been used to monitor hot-carrier relaxation in carbon nanotubes [30] and does not include radiation.

The computational conditions were as follows. The plane wave basis set with a cutoff energy of 64 Ry and the norm-conserving pseudopotentials [31] were used for expressing valence electrons and their interactions with ions, respectively. The local density approximation (LDA) was employed for the exchange-correlation potential, and the functional form for the electron gas [32] was used. In this work, the functional within the generalized gradient approximation has not been tested as it gave a bit larger lattice constant of diamond with use of currently employed pseudopotentials. Thus, the choice of LDA is practical. The model of the diamond divacancy was a supercell containing 216 carbon (C) atoms ( $3 \times 3 \times 3$  of the cubic cell) from which two neighboring C atoms were removed to form a divacancy. The spin-unpolarized approximation with fractional numbers was used for electron occupation [33,34]. The choice of spin-unpolarized approximation cannot provide enough results to compare the computed electronic structure with electron spin resonance data, which is beyond current scope. However, this approximation works well for relaxation dynamics of excited state within the time-scale of a few hundred fs, at which contribution of spin is negligibly small. A  $\Gamma$  point was used for sampling in the momentum space.

The atomic geometry was optimized in the electronic ground state and neutral charge state. When the simulation of real-time electron-ion dynamics was started by promoting electrons, randomized initial velocities were given to all ions to mimic the Boltzmann distribution at the lattice temperature of 10 K. Owing to computational costs, a low lattice temperature was used to avoid large variation in the velocity of each atom. The decay process at room temperature should also be studied, although this requires ensemble dynamics with many different sets of randomized initial velocities due to the large variation in velocities. The current approach, assuming a low temperature, corresponds to a practical situation in which optical spectroscopy is performed at cryogenic temperatures [20].

The Suzuki-Trotter split operator scheme [35,36] was used for the time integration of the time-dependent Kohn-Sham equation (1). The interval of the time-step for electron-ion

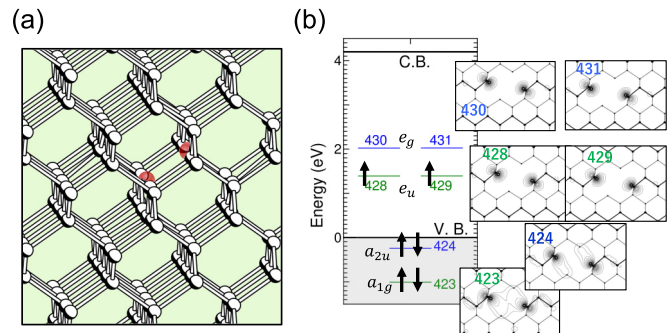


FIG. 1. (a) Atomic structure of the divacancy. Red transparent balls denote positions of two vacancies in nearest neighbor sites. Other open balls are carbon atoms. (b) Energy levels of divacancy-related states. Possible spin configuration is denoted by arrows, but the current computation was within the spin-unpolarized approximation. “C. B.” should read “Conduction band” and “V. B.” should read “Valence band.” Numbers 423, 424, and 428–431 are band indices of states localized at the divacancy, as denoted in the contour maps of the norm of each wave function. Sixteen contour lines are drawn with intervals of  $6.68 \times 10^{-4} e/r_0^3$  for band 423 ( $a_{1g}$ ),  $1.23 \times 10^{-3} e/r_0^3$  for band 424 ( $a_{2u}$ ),  $8.57 \times 10^{-4} e/r_0^3$  for band 428 ( $e_u$ ),  $2.78 \times 10^{-3} e/r_0^3$  for band 429 ( $e_u$ ),  $9.30 \times 10^{-4} e/r_0^3$  for band 430 ( $e_g$ ), and  $2.97 \times 10^{-3} e/r_0^3$  for band 431 ( $e_g$ ). For a unit  $e/r_0^3$ ,  $e$  is the electron charge, and  $r_0$  is the Bohr radius.

dynamics was set to 0.03 atomic units (0.726 as). Computational code FPSEID<sup>21</sup> [37] was used which was developed with numerical schemes [38,39].

### III. RESULTS

#### A. Atomic and electronic structures of the divacancy

Figure 1(a) shows the atomic configuration of the divacancy obtained by the current computational scheme in the electronic ground state. There were two vacancies at nearest-neighbor sites ( $D_{3d}$  symmetry configuration) causing doubly degenerate electronic levels in the diamond bandgap [Fig. 1(b)]. Conversely, a calculation using the HSE06 functional [40,41] gave the two nearest vacancies with  $C_{2h}$  symmetry with total energy 0.07 eV lower than that of  $D_{3d}$  symmetry [42], and there has been an experimental report proposing the vacancies have  $C_{2h}$  symmetry [43]. However, implementation of the HSE06 or other hybrid functional in the real-time propagation schemes was not feasible for the current model size and purpose. Therefore, the  $D_{3d}$  atomic configuration obtained by the LDA functional was used as a compromise as a test case to study the decay process of the optically excited state.

Figure 1(b) shows the electronic levels obtained by DFT calculations. The numbers indicate the band indices of the supercell, and the bands at 423 ( $a_{1g}$ ), 424 ( $a_{2u}$ ), and from 428 to 431 ( $e_u$  and  $e_g$ ) are divacancy-related states, which were confirmed by analyzing the characteristics of each wave function, shown as panels with corresponding band indices. The panels show contour maps of the norm of each wave function on the (110) plane containing the divacancy. Within the spin-unpolarized approximation, bands 428/429 ( $e_u$ ) and 430/431 ( $e_g$ ) were doubly degenerate, and thus bands 428/429 had an

occupation per spin of 0.5. The optical transition from band 423 to bands 428/429 ( $a_{1g} \rightarrow e_u$ ) was allowed according to the computed dipole matrix. Similarly, the transition from band 424 to bands 430/431 ( $a_{2u} \rightarrow e_g$ ) was also allowed.

The excitation energy computed with the  $\Delta$ SCF scheme promoting a single electron from band 423 to bands 428/429 ( $a_{1g} \rightarrow e_u$ ) was 2.44 eV with a corresponding wave length of 508 nm. (For details in assigning the occupation numbers for the ground and excited states, please see Table S.I in the Supplemental Material [44]). After the promotion, the occupation per spin was 0.5 for band 423, and 0.75 for bands 428/429 in the current approximation. The  $\Delta$ SCF calculation for another excitation path (from band 424 to bands 430/431) ( $a_{2u} \rightarrow e_g$ ) suggested that the characteristics of the hole wave function changed from band 424 to band 426 during the SCF loop. Therefore, electron promotion was modified to excitation from band 426 to bands 430/431 to complete the  $\Delta$ SCF calculation, and the computed optical excitation was 2.32 eV with a corresponding wave length of 534 nm. Here, the electron promotion should be an occupation per spin of 0.5 for band 426, and 0.25 for each of bands 430/431, by keeping 0.5 electrons per spin for each of bands 428/429. However, to obtain convergence in the  $\Delta$ SCF calculation, the occupation per spin was changed from 0.5 to 0.6 for band 426 and from 1.0 to 0.9 for band 427, which is just above band 426. The current  $\Delta$ SCF approximation gave optical excitation energies for the two paths as 2.44 eV and 2.32 eV, meanwhile the absorption energy mentioned in [24] was around 2.5 eV. The close values between current calculations and the experiment look surprisingly good despite the common trend of the underestimation of excitation energy by DFT, while it should be noted that current model of divacancy is under  $D_{3d}$  symmetry while the experimental one could be under  $C_{2v}$  symmetry as was discussed in the beginning in this subsection.

### B. Dynamics in the divacancy in the photoexcited state

With an initial condition prepared by promoting electron occupation from band 423 to bands 428/429 ( $a_{1g} \rightarrow e_u$ ), the electron-ion dynamics were calculated by TDDFT at a lattice temperature of 10 K with randomized ions' velocities. Figure 2(a) shows the time evolution of the expectation values of the time-dependent Kohn-Sham orbitals. Level crossing between bands 423 and 428 was seen after 200 fs. The expectation values of the fully occupied band (back lines) and half-occupied and three-quarter occupied bands (green lines) crossed to each other. To reproduce these electron dynamics by performing conventional MD based on static DFT, the occupation numbers must be redistributed to mimic the level alternation by carefully monitoring the level crossing throughout the MD simulation, although this is difficult practically for extended systems. Around 400 fs, bands 423, 428, and 429 had similar energy levels. At this time, the wave function characteristics for band 423 started to change, and they had changed greatly at  $t = 400$  fs (contour map shown in the inset). Initially, the characteristics of band 423 ( $a_{1g}$ ) were the same as those of band 423 [Fig. 1(b)], whereas around 400 fs, the characteristics became similar to those of bands 428/429 ( $e_u$ ) [Fig. 1(b)].

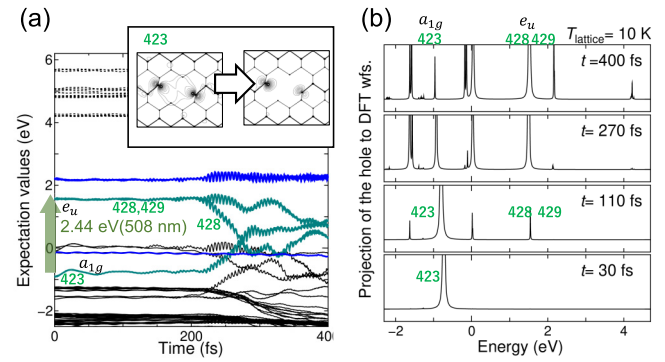


FIG. 2. Time evolution of the photogenerated hole's wave function. (a) Expectation values over time. Green lines show excitation paths from band 423 to bands 428/429 ( $a_{1g} \rightarrow e_u$ ). The vertical green arrow denotes the excitation path and energy. Blue curves show the other pair of excitation paths. The inset shows the change in characteristics of the norms of the hole's wave function of band 423 at the beginning and end of the simulation. Sixteen contour lines are drawn with an interval of  $1.23 \times 10^{-3} e/r_0^2$  at the beginning and with an interval of  $7.21 \times 10^{-3} e/r_0^3$  at  $t = 400$  fs. Here,  $e$  and  $r_0$  are the electron charge and Bohr radius, respectively. (b) Profile of projection  $P(\epsilon, t)$  (vertical axis) as a function of electron energy level  $\epsilon$  (lateral axis) at  $t = 30, 110, 270,$  and  $400.7$  fs. The band indices determined by static DFT calculations are also shown.

Because it may be ambiguous to discuss similarities in the norm of the wave functions only from contour maps, a semiquantitative analysis was performed to take the projection of band 423 of

$$P(\epsilon, t) = \frac{1}{\pi} \text{Im} \sum_m \frac{|\langle \psi_{423}^{\text{TDDFT}}(\mathbf{r}, t) | \psi_m^{\text{DFT}}(\mathbf{r}) \rangle|^2}{\epsilon - \epsilon_m - i0^+}, \quad (3)$$

where  $\epsilon$  is an electron energy level and  $\psi_m^{\text{DFT}}(\mathbf{r})$  is Kohn-Sham orbital of band  $m$  obtained by static DFT with corresponding Kohn-Sham level  $\epsilon_m$ . The value of  $0^+$  (broadening factor) was set as 3.5 meV. Figure 2(b) shows the plot of  $P(\epsilon, t)$  at  $t = 30, 110, 270,$  and  $400$  fs. The atomic coordinates of electron-ion dynamics at each time were used to perform the static DFT calculation to obtain  $\psi_m^{\text{DFT}}(\mathbf{r})$ . Initially, the projection had a sharp peak at the energy level of band 423 ( $a_{1g}$ ). However, after 400 fs, the projection showed a distribution with many peaks, including the projection to bands 428/429 ( $e_u$ ) in addition to the valence and conduction bands of diamond obtained by static DFT. This indicates that the main characteristics of the wave function of the hole changed to excited electrons, suggesting that direct electron-hole recombination without radiation occurred.

Next, we focused on the other path of optical excitation ( $a_{2u} \rightarrow e_g$ ). Performing the  $\Delta$ SCF calculation to prepare the initial conditions changed the excitation from band 424 to bands 430/431, to excitation from band 426 to bands 430/431 at the end of the SCF convergence. Figure 3 shows relaxation dynamics after this excitation. Up to 500 fs, no major changes in the expectation values were observed [Fig. 3(a)]. The inset in Fig. 3(a) shows the time evolution of the wave function characteristics as contour maps of the norm of the wave function of band 426. The contour maps showed almost

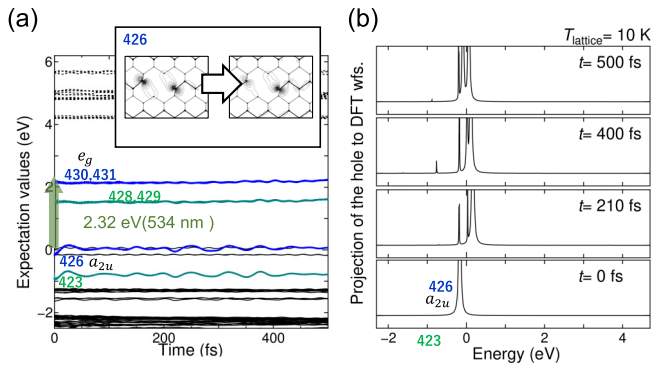


FIG. 3. (a) Same as Fig. 2(a) but after excitation from band 426 to bands 430/431 ( $a_{2u} \rightarrow e_g$ ) (blue curves). The vertical green arrow denotes the excitation path and energy. The inset shows contour maps of the time evolution of the wave function characteristics of band 426. Sixteen contour lines with intervals of  $1.26 \times 10^{-3} e/r_0^3$  were drawn for the initial contour map, whereas for  $t = 500$  fs, the interval was  $8.40 \times 10^{-4} e/r_0^3$ , where  $e$  and  $r_0$  are the electron charge and Bohr radius, respectively. (b) Same as Fig. 2(b) but after excitation from band 426 to bands 430/431. The projection of the time-evolving wave function of band 426 is plotted at 0, 210, 400, and 500 fs.

no change, indicating that the lifetime without nonradiative decay should be longer than 500 fs, and could result in high light emission efficiency. However, more detailed analysis by taking the projection of a wave function of band 246 to wave functions obtained by static DFT [Eq. (3)] suggested that the hybridization of orbitals near the edge of the valence bands with band 426 [Fig. 3(b)]. Therefore, the oscillator strength for the optical transition from bands 430/431 ( $e_g$ ) to band 426 ( $a_{2u}$ ) should be decreased, whereas the evaluation of the dipole matrix element was complex because the wave functions evolve over time and applying the Fermi-golden rule by using the dipole matrix element was inappropriate on the short time scale in this work.

It is of fundamental interest whether the divacancy is detectable by measuring the light emission after photoexcitation. The two excitation paths had similar excitation energy within current computational precision, and one of the two paths showed rapid nonradiative decay, even at a lattice temperature of 10 K. If the present calculation of excitation energy were a good approximation, it would be likely to excite two paths simultaneously, causing an increase in lattice temperature due to the fast nonradiative decay in one of the two excitation paths. If this were the case, light emission from the other excitation path would be disturbed.

### C. Effect of H termination on one dangling bond in the divacancy

Since chemical vapor deposition is used for diamond growth, hydrogen (H) contamination is inevitable as the source gas (methane) contains H atoms. Indeed, H contamination was reported to deactivate their optical activity of NV center [45]. Such hydrogen contamination could also be the case during the formation of the divacancy. One of the excitation paths is terminated when an H atom is captured by the divacancy. Figure 4(a) shows the optimized structure in the electronic ground state in the current computational

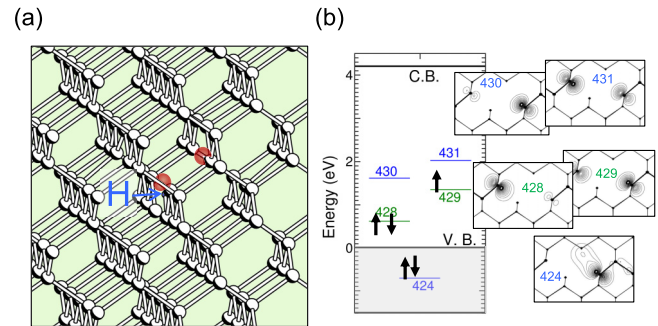


FIG. 4. (a) Atomic structure of H-terminated divacancy. Red transparent circles denote positions of two vacancies at nearest-neighbor sites. Small blue circle indicated by the arrow is a hydrogen atom. Other open circles are carbon atoms. (b) Energy levels of divacancy-related states. The possible spin configuration is denoted by arrows but the current computation was within the spin-unpolarized approximation. “C. B.” should read “Conduction band” and “V. B.” should read “Valence band.” Labels 424 and 428 to 431 are the band indices of states localized at the divacancy, as shown by the contour maps indicating the norm of each wave function (see main text). Sixteen contour lines are drawn with intervals of  $1.51 \times 10^{-3} e/r_0^3$  for band 424,  $3.12 \times 10^{-3} e/r_0^3$  for band 428,  $3.25 \times 10^{-3} e/r_0^3$  for band 429,  $1.74 \times 10^{-3} e/r_0^3$  for band 430, and  $3.35 \times 10^{-3} e/r_0^3$  for band 431.  $e$  is the electron charge and  $r_0$  is the Bohr radius.

schemes. The energy level diagram in Fig. 4(b) is similar to that in Fig. 1(b), although band 423 is not displayed because this band becomes a diamond bulk valence band due to H-C bonding lowering the energy level of the original band 423. Because of the presence of the H atoms, the  $D_{3d}$  symmetry was broken, and thus degenerate bands 428/429 ( $e_u$ ) and 430/431 ( $e_g$ ) were split. Arrows indicate the possible spin configuration, but the current calculation was done within the spin-unpolarized approximation. According to the calculated dipole matrix elements, the possible optical transition was from band 424 to bands 430 and 431. Here, we focused on the excitation from bands 424 to 430 because the matrix elements of this excitation had larger values.

We examined the electron-ion dynamics after promotion of single electron excitation from band 424 to band 430 by keeping the occupation of band 429 as 0.5 at a lattice temperature of 10 K. (For details in assigning the occupation numbers for the ground and excited states, please see Table S.II in the Supplemental Material [44]). Figure 5 shows the results. The splitting of expectation values of bands 430 and 431 became narrow because the electronic level of band 430 increased with increased electron occupation. Figure 5(a) shows the time evolution of the expectation values, which oscillated at a higher frequency compared with those in Fig. 3(a). The higher frequency arose from the vibration of the C-H bonds, which caused substantial dynamic perturbation of the Hamiltonian because the H atom was positively charged due to its smaller electron affinity than the C atoms. The wave function characteristics of band 424 showed a large change [inset of Fig. 5(a)]; the wave function was initially localized at the dangling bond, whereas it had spread to entire unit cells at  $t = 400$  fs.

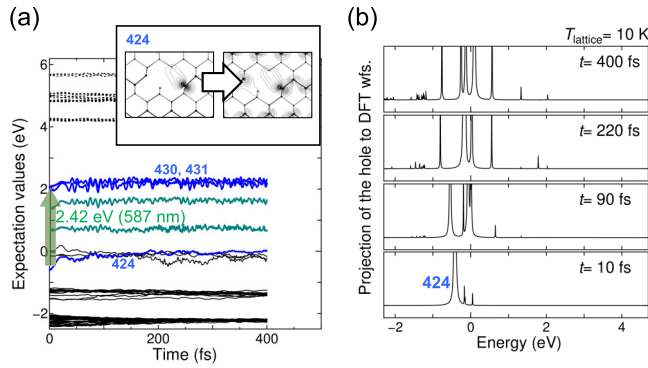


FIG. 5. (a) Time evolution of expectation values of the time-dependent Kohn-Sham wave functions after excitation from band 424 to band 430 (blue curves). The vertical green arrow denotes the excitation path and energy. The inset shows contour maps of the time evolution of the wave function characteristics of band 424. Sixteen contour lines with intervals of  $1.42 \times 10^{-3} e/r_0^3$  were drawn for the initial contour map, whereas for  $t = 400$  fs, the interval was  $4.50 \times 10^{-5} e/r_0^3$ , where  $e$  and  $r_0$  are the electron charge and Bohr radius, respectively. (b) Projection of wave function of band 424 to those obtained by static DFT with atomic coordinates at snapshots of  $t = 10, 90, 220,$  and  $400$  fs.

The spread was also observed in the time evolution of the projection of the wave function of band 424 to those obtained by static DFT [Fig. 5(b)]. The peak of the original band 424 was split into many sharp peaks in the valence bands. This process did not correspond to electron-hole direct recombination but to fast delocalization of the photogenerated hole in the valence bands. Therefore, light emission after decay should not be expected in this case.

#### IV. CONCLUSIONS

First-principles simulations of electron-ion dynamics within TDDFT were performed to study the relaxation process of optically excited divacancies in diamond. A model with two neighboring C atom vacancies was used and two excitation paths were found by analyzing the wave function characteristics and the dipole matrix obtained by using static DFT calculations to prepare the initial conditions for TDDFT simulations. The TDDFT simulations revealed simultaneous nonradiative decay with electron-hole direct recombination in one of the two optical excitation paths at a lattice temperature of 10 K, whereas the other optical excitation path showed weakening of the emission intensity.

The present results should be compared with the optical properties of the NV and IV-V centers. In particular, the level structure shown in Fig. 1(a) was similar to that of the IV-V center, except for the electron occupations. In both systems, there are two sets of doubly degenerate states in the bandgap

of diamond within the spin-unpolarized approximation. For the IV-V center, the lower doubly degenerate states are fully occupied and may be just below the valence top [16,18]. The similarity was due to the  $D_{3d}$  symmetry in our divacancy model, which is a proposed symmetry for the IV-V center. The excitation path from band 426 to bands 430/431 of Fig. 3(a) ( $a_{2u} \rightarrow e_g$ ) was similar to that of the IV-V center. In contrast to the IV-V center, the divacancy has no ions in the middle of the two vacancy sites, causing a difference in the degree of freedom for lattice motion. In this case, the weakening of the oscillator strength through the electron-ion interaction is greater in the divacancy than that in the IV-V center. For the excitation path from band 423 to bands 428/429 [Fig. 2(a)] ( $a_{1g} \rightarrow e_u$ ), the corresponding levels in the IV-V center are fully occupied, and thus no excitation is allowed.

The calculated excitation energies of the two excitation paths in the divacancy are 2.3 to 2.4 eV, which corresponds to a green emission and are similar to that from NV centers (2.16 eV in the neutral charge state) [12]. The computed excitation energy is always underestimated; therefore, the difference in the excitation energy of the divacancy and the NV center should be larger and distinguishable. However, the TDDFT calculations suggested that nonradiative decay occurred and the emission strength from the divacancy was weakened, and consequently, it is unlikely that the divacancy could be detected by light emission. Moreover, the simulation of the effect of partial termination of the C-dangling bond with an H atom showed nonradiative decay that delocalized the excited hole state into the diamond valence bands; thus, H termination did not change the undetectable nature of divacancy by light emission. The charged states of the divacancy have not been studied, but they are likely to exhibit nonradiative decay of the excited state or rapid weakening of the light emission.

These findings suggest that the divacancy under the  $D_{3d}$  symmetry is not suitable for optical devices, although our work has provided insights into understanding some potential roles of divacancies, especially their influence on color centers in diamond. Finally, we note that the current TDDFT calculations did not include the excitonic effect, namely electron-hole interactions under optical excitation. Whether the excitonic effect is strong enough to suppress the nonradiative decay is a fundamental question.

#### ACKNOWLEDGMENTS

The author thanks Dr. T. Iwasaki for fruitful discussions. This work is financially supported by JSPS KAKENHI Grant No. JP22H04962 and MEXT Quantum Leap Flagship Program (MEXT Q-LEAP) Grant No. JPMXS0118067395. All calculations were performed using the supercomputer at the Tohoku University Cyberscience Center.

[1] I. A. Buyanova, W. M. Chen, G. Pozina, B. Monemar, W.-X. Ni, and G. V. Hansson, Mechanisms for thermal quenching of luminescence in sige/si structures grown by molecular beam epitaxy: Role of nonradiative defects, *Appl. Phys. Lett.* **71**, 3676 (1997).

[2] S. Roy, W. Choi, S. Jeon, D.-H. Kim, H. K. S. J. Yun, Y. Lee, J. Lee, Y.-M. Kim, and J. Kim, Atomic observation of filling vacancies in monolayer transition metal sulfides by chemically sourced sulfur atoms, *Nano Lett.* **18**, 4523 (2018).

- [3] S. F. Chichibu, A. Uedono, K. Kojima, H. Ikeda, K. Fujito, S. Takashima, M. Edo, K. Ueno, and S. Ishibashi, The origins and properties of intrinsic nonradiative recombination centers in wide bandgap gan and algan, *J. Appl. Phys.* **123**, 161413 (2018).
- [4] P. Tatarczak, H. Turski, K. P. Korona, E. Grzanka, C. Skierbiszewski, and A. Wyszomolka, Optical properties of n-polar gan; the possible role of nitrogen vacancy-related defects, *Appl. Surf. Sci.* **566**, 150734 (2021).
- [5] A. Alkauskas, Q. Yan, and C. G. VandeWalle, First-principles theory of nonradiative carrier capture via multiphonon emission, *Phys. Rev. B* **90**, 075202 (2014).
- [6] M. E. Turiansky, A. Alkauskas, M. Engel, G. Kresse, D. Wickramaratne, J.-X. Shen, C. Dreyer, and C. G. V. de Walle, Nonrad: Computing nonradiative capture coefficients from first principles, *Comput. Phys. Commun.* **267**, 108056 (2021).
- [7] R. T. Harley, M. J. Henderson, and R. M. Macfarlane, Persistent spectral hole burning of color centers in diamond, *J. Phys. C: Solid State Phys.* **17**, L233 (1984).
- [8] Y. Yokota, J. S. Ma, T. Ito, A. Hiraki, A. Kurita, and T. Kushida, Persistent hole burning of the nitrogen vacancy center and the 2.16 eV center of chemical-vapor deposited diamond, *Appl. Phys. Lett.* **61**, 2138 (1992).
- [9] H. Hanzawa, Y. Nishida, and T. Kato, Measurement of decay time for the NV centre in Ib diamond with a picosecond laser pulse, *Diam. Relat. Mater.* **6**, 1595 (1997).
- [10] C. Kurtsiefer, S. Mayer, P. Zarda, and H. Weinfurter, Stable Solid-State Source of Single Photons, *Phys. Rev. Lett.* **85**, 290 (2000).
- [11] S. Pezzagna, D. Rogalla, D. Wildanger, H. Meijer, and A. Zaitsev, Creation and nature of optical centres in diamond for single-photon emission-overview and critical remarks, *New J. Phys.* **13**, 035024 (2011).
- [12] N. Mizuochi, T. Makino, H. Kato, D. Takeuchi, M. Ogura, H. Okushi, M. Nothaft, P. Neumann, A. Gali, F. Jelezko, J. Wrachtrup, and S. Yamasaki, Electrically driven single-photon source at room temperature in diamond, *Nat. Photon.* **6**, 299 (2012).
- [13] M. Haruyama, H. Kato, M. Ogura, Y. Kato, D. Takeuchi, S. Yamasaki, T. Iwasaki, M. Morishita, M. Fujiwara, N. Mizuochi, and T. Makino, Electroluminescence of negatively charge single NV centers in diamond, *Appl. Phys. Lett.* **122**, 072101 (2023).
- [14] C. Wang, C. Kurtsiefer, H. Weinfurter, and B. Burchard, Single photon emission from SiV centres in diamond produced by ion implantation, *J. Phys. B: At. Mol. Opt. Phys.* **39**, 37 (2006).
- [15] A. Sipahigil, K. D. Jahnke, L. J. Rogers, T. Teraji, J. Isoya, A. S. Zibrov, F. Jelezko, and M. D. Lukin, Indistinguishable Photons from Separated Silicon-Vacancy Centers in Diamond, *Phys. Rev. Lett.* **113**, 113602 (2014).
- [16] T. Iwasaki, F. Ishibashi, Y. Miyamoto, Y. Doi, S. Kobayashi, T. Miyazaki, K. Tahara, K. D. Jahnke, L. J. Rogers, B. Naydenov, F. Jelezko, S. Yamasaki, S. Nagamachi, T. Inubushi, N. Mizuochi, and M. Hatano, Germanium-vacancy single color centers in diamond, *Sci. Rep.* **5**, 12882 (2015).
- [17] T. Iwasaki, Y. Miyamoto, T. Taniguchi, P. Siyushev, M. H. Metsch, F. Jelezko, and M. Hatano, Tin-Vacancy Quantum Emitters in Diamond, *Phys. Rev. Lett.* **119**, 253601 (2017).
- [18] G. Thiering and A. Gali, *Ab Initio* Magneto-Optical Spectrum of Group-IV Vacancy Color Centers in Diamond, *Phys. Rev. X* **8**, 021063 (2018).
- [19] J. Görlitz, D. Herrmann, P. Fuchs, T. Iwasaki, T. Taniguchi, D. Rogalla, D. Hardeman, P.-O. Colard, M. Markham, M. Hatano, and C. Becher, Coherence of a charge stabilized tin-vacancy spin in diamond, *npj Quantum Inf.* **8**, 45 (2022).
- [20] Y. Narita, P. Wang, K. Ikeda, K. Oba, Y. Miyamoto, T. Taniguchi, S. Onoda, M. Hatano, and T. Iwasaki, Multiple Tin-Vacancy Centers in Diamond with Nearly Identical Photon Frequency and Linewidth, *Phys. Rev. Appl.* **19**, 024061 (2023).
- [21] M. A. Lea-Wilson, J. N. Lomer, and J. A. van Wyk, Electron spin resonance of the R4/W6 defect in irradiated diamond, *Phil. Mag. B* **72**, 81 (1995).
- [22] J. M. Baker, Deducing atomic model for point defect in diamond: The relevance of their mechanisms of formation, *Diam. Relat. Mater.* **16**, 216 (2007).
- [23] B. Slepetz and M. Kertesz, Divacancies in diamond: A stepwise formation mechanisms, *Phys. Chem. Chem. Phys.* **16**, 1515 (2014).
- [24] J. W. Steed and S. Kohn, Annealing of electron radiation damage in a wide range of Ib and Iia diamond samples, *Diam. Relat. Mater.* **50**, 110 (2014).
- [25] E. Runge and E. K. U. Gross, Density-Functional Theory for Time-Dependent Systems, *Phys. Rev. Lett.* **52**, 997 (1984).
- [26] P. Hohenberg and W. Kohn, Inhomogeneous electron gas, *Phys. Rev.* **136**, B864 (1964).
- [27] W. Kohn and L. Sham, Self-consistent equations including exchange and correlation effects, *Phys. Rev.* **140**, A1133 (1965).
- [28] P. Ehrenfest, Remark about the approached validity of the classic mechanics within the quantum mechanics, *Z. Phys.* **45**, 455 (1927).
- [29] J. Ihm, A. Zunger, and M. L. Cohen, Momentum space formalism for the total energy of solids, *J. Phys. C: Solid State Phys.* **12**, 4409 (1979).
- [30] Y. Miyamoto, A. Rubio, and D. Tománek, Real-Time *Ab Initio* Simulations of Excited Carrier Dynamics in Carbon Nanotubes, *Phys. Rev. Lett.* **97**, 126104 (2006).
- [31] N. Troullier and J. L. Martins, Efficient pseudopotentials for plane-wave calculations, *Phys. Rev. B* **43**, 1993 (1991).
- [32] J. P. Perdew and A. Zunger, Self-interaction correction to density-functional approximation for many-electron systems, *Phys. Rev. B* **23**, 5048 (1981).
- [33] M. Weinert and J. W. Davenport, Fractional occupations and density-functional energies and forces, *Phys. Rev. B* **45**, 13709 (1992).
- [34] A. Alavi, J. Kohanoff, M. Parrinello, and D. Frenkel, *Ab Initio* Molecular Dynamics with Excited Electrons, *Phys. Rev. Lett.* **73**, 2599 (1994).
- [35] M. Suzuki, General nonsymmetric higher-order decomposition of exponential operators and symplectic integration, *J. Phys. Soc. Jpn.* **61**, 3015 (1992).
- [36] M. Suzuki and T. Yamauchi, Convergence of unitary and complex decompositions of exponential operators, *J. Math. Phys.* **34**, 4892 (1993).
- [37] The fpseid<sup>21</sup> official website, (fpseid<sup>21</sup> ©AIST 2021) (2022), [https://staff.aist.go.jp/yoshi-miyamoto/index\\_en.html](https://staff.aist.go.jp/yoshi-miyamoto/index_en.html).
- [38] O. Sugino and Y. Miyamoto, Density-functional approach to electron dynamics: Stable simulation under a self-consistent field, *Phys. Rev. B* **59**, 2579 (1999).
- [39] O. Sugino and Y. Miyamoto, Erratum: Density-functional approach to electron dynamics: Stable simulation under a

- self-consistent field [Phys. Rev. B 59, 2579 (1999)], *Phys. Rev. B* **66**, 089901(E) (2002).
- [40] J. Heyd, G. E. Scuseria, and M. Ernzerhof, Hybrid functionals based on a screened Coulomb potential, *J. Chem. Phys.* **118**, 8207 (2003).
- [41] A. V. Krukau, O. A. Vydrov, A. F. Izmaylov, and G. E. Scuseria, Influence of the exchange screening parameter on the performance of screened hybrid functionals, *J. Chem. Phys.* **125**, 224106 (2006).
- [42] P. Deák, B. Aradi, M. Kaviani, T. Frauenheim, and A. Gali, Formation of NV centers in diamond: A theoretical study based on calculated transition and migration of nitrogen and vacancy related defects, *Phys. Rev. B* **89**, 075203 (2014).
- [43] D. J. Twitchen, M. E. Newton, J. M. Baker, T. R. Anthony, and W. F. Banholzer, Electrons-paramagnetic-resonance measurements on the divacancy defect center R4/W6 in diamond, *Phys. Rev. B* **59**, 12900 (1999).
- [44] See Supplemental Material at <http://link.aps.org/supplemental/10.1103/PhysRevMaterials.7.086002> for Table of occupation numbers assigned on each band for calculating ground and excited states.
- [45] A. Stacey, T. J. Karle, J. P. McGuinness, B. C. Gibson, K. Ganesan, S. Tomljenovic-Hanic, A. D. Greentree, A. Hoffman, R. G. Beausoleil, and S. Praver, Depletion of nitrogen-vacancy color centers in diamond via hydrogen passivation, *Appl. Phys. Lett.* **100**, 071902 (2012).